



The new polymict eucrite Dar al Gani 983: Petrography, chemical composition, noble gas record, and evolution

Andrea PATZER^{1*}, Jochen SCHLÜTER², Ludolf SCHULTZ³, Dolores H. HILL¹, and William V. BOYNTON¹

¹Lunar and Planetary Laboratory, University of Arizona, Tucson, Arizona 85721, USA

²Mineralogisches Museum der Universität Hamburg, D-20146 Hamburg, Germany

³Max-Planck-Institut für Chemie, D-55020 Mainz, Germany

*Corresponding author. E-mail: apatzer@lpl.arizona.edu

(Received 24 September 2004; revision accepted 07 April 2005)

Abstract—Mineralogical and chemical studies of Dar al Gani 983 show that this meteorite is a eucrite. Its texture is that of an impact breccia. It contains cumulate pyroxene and feldspar megacrysts, a variety of recrystallized melt clasts, clasts of subophitic basalt, and mesostasis. These components are embedded in a matrix of fragmental pyroxene and plagioclase. In addition, the entire rock is penetrated by glassy melt veins and patches, and displays features of strong shock.

The mineralogical and chemical evidence obtained for DaG 983 indicates that this meteorite experienced a complex evolutionary history. The presence of cumulate silicate crystals implies substantial, large scale cratering events on the HED asteroid. As a result of these impacts, rocks from different intrusive bodies to extrusive surface layers were laterally and vertically transported to form a thoroughly mixed megaregolith. DaG 983 represents a sample of this megabreccia.

INTRODUCTION

Eucrites are differentiated achondrites and share a common provenance with howardites and diogenites (e.g., Tschermak 1885; Stolper 1977; Clayton and Mayeda 1996). Eucrite mineralogical composition is basaltic. The howardite-eucrite-diogenite (HED) suite is unique among meteorite chemical associations in that it is almost certainly linked to a specific asteroid, 4 Vesta (see Drake 2001, and references therein).

Eucrites can be subdivided into noncumulate, cumulate, and polymict types. The noncumulate eucrites are further subdivided into three different compositional series: main group; Stannern trend; and Nuevo Laredo trend. These subtypes are classified by their mg# and Ti contents (BVSP 1981).

Considerable work has addressed the metamorphism and impact heating of eucrites (e.g., Nyquist et al. 1986, 1997; Takeda and Graham 1991; Metzler et al. 1995; Takeda 1997; Yamaguchi et al. 1997a, 2001). Almost all eucritic samples show signs of thermal overprinting and many breccias formed by impact mixing. It has been demonstrated that the bombardment history of the HED parent body equals the Moon's in complexity (Bogard 1995).

Our work focuses on the petrographic description of a new eucrite from Libya, Dar al Gani (DaG) 983. We also

provide an outline of the geological settings involved in its formation. Our constraints on the evolutionary path of this meteorite were derived from electron microprobe, instrumental neutron activation analysis (INAA), and noble gas data (for noble gas data see Patzer et al. 2003a).

SAMPLE AND ANALYTICAL TECHNIQUES

Sample

DaG 983 was recovered during a German-Libyan expedition (J. Schlüter and F. Thiedig, Hamburg; L. Schultz, Mainz; Abd Elfatah M. Abu-Aghreb, Tripoli) from the Dar al Gani Plateau in Libya in March 2002 (Schlüter et al. 2002). It was found as a single stone of 933 g partly covered with black fusion crust. The interior of the rock is light grey in color, displaying open cracks and some melt veins with microscopic vesicles. Occasionally, the cracks and vesicles contain white aggregates of gypsum or calcite. The meteorite's texture is that of a breccia with relatively large light and dark clasts being embedded in a fine-grained fragmental matrix (Fig. 1; see Russell et al. 2003).

Petrography, Bulk, and Mineral Analyses

Two thin sections of DaG 983 (adjacent faces within

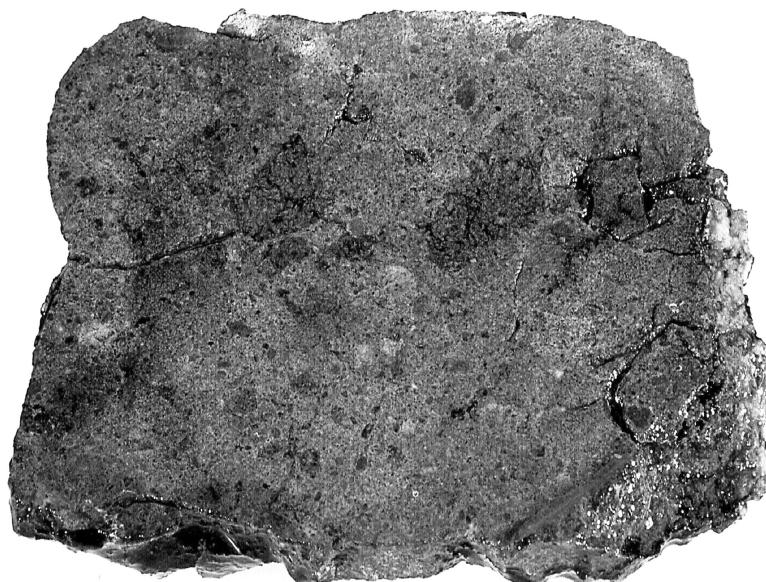


Fig. 1. The interior of the DaG 983 polymict eucrite appears unaltered. The influence of weathering, however, is obvious from a few cracks and vesicles that are filled with terrestrial gypsum and calcite microcrystals. The brecciated character of the sample is readily noticeable. Some clasts measure up to 10 mm (the slab has a size of about 50×70 mm; photo taken by K. C. Lyncker).

~ 2 mm) were prepared for optical microscope studies and electron microprobe measurements. The chemical analyses of the meteorite's mineral components were, in part, carried out with a Cameca Camebax SX 100 Microbeam wavelength-dispersive electron microprobe at the Department for Mineralogy and Petrology of the Universität Hamburg. Operation conditions were set to 20 kV and 25 nA. For all elements, the $K\alpha$ X-ray line was applied. Pure elements (Ni and Co), andradite (for Ca and Si), apatite (for P), vanadinite (for V), as well as synthetic MgO (for Mg), Al_2O_3 (for Al), ZnS (for Zn and S), $MnTiO_3$ (for Ti and Mn), Cr_2O_3 (for Cr), and FeS_2 (for Fe) were used as standards. Additional comprehensive analyses were conducted with a Cameca SX-50 electron microprobe at the Lunar and Planetary Laboratory, Tucson, Arizona. This microprobe study included major element quantification, backscattered electron imaging, and X-ray mapping. An accelerating voltage of 15 kV, a sample current of 20 nA, and 20 sec peak count times were applied for all analyses. Natural and synthetic standards were used (see Kring et al. 1996). All data (Hamburg and Tucson) were corrected for absorption, fluorescence, and atomic number effects based on the correction method introduced by Pouchon and Pichoir (1991). The elemental compositions of the major and minor mineral phases are listed in Tables 1a and 1b.

For the INAA, three chips of 0.174, 0.147, and 0.185 g were broken off of a subsample. The 0.185 g-aliquant contained a macroscopically notable dark clast. The irradiation took place at the reactor facility (TRIGA) of the University of Arizona. The specimens were first exposed to a high flux ("rabbit") irradiation for 60 seconds followed by a 3-hour (lazy susan) irradiation. Irradiations included both

synthetic standards and standard rocks. Details on the irradiation procedure and used standards have been reported by Patzer et al. (2004). Elemental concentrations of the samples were determined by the comparator method. The samples experienced a neutron flux of 6.3×10^{13} n/cm² in the rabbit and 7.56×10^{15} n/cm² in the lazy susan run. Table 2 shows the bulk elemental concentrations obtained by INAA.

RESULTS AND DISCUSSION

Weathering Degree, Shock Stage, and Petrographic Description

The occurrence of secondary gypsum and carbonate microcrystals in cracks and vesicles of DaG 983 indicates that the meteorite is slightly altered by terrestrial weathering (the Dar al Gani meteorite field in Libya is situated on Tertiary dolomites and limestone) (Schlüter et al. 2002).

The presence of heavily fractured mineral phases and strong mosaicism suggest that DaG 983 is severely shocked. Most of the plagioclase has been converted into maskelynite. Abundant glassy melt veins crosscut the rock. In addition, some pyroxenes appear to show signs of incipient decomposition or melting. According to the criteria of Stöffler et al. (1988), the shock features observed in DaG 983 are stage 2b.

Petrographically, DaG 983 belongs to the polymict breccias. It is composed of four different types of clasts that are embedded in a fragmental groundmass of variably coarse-grained pyroxene and plagioclase. Clast types include predominant monomineralic pyroxene and feldspar megacrysts, recrystallized melt pockets, and basaltic

Table 1a. Chemical composition of selected silicate phases in DaG 983 (av. ox%).

	Plagioclase megaclasts	Plagioclase melt pockets	Plagioclase spinfex melt	Pigeonite megaclasts	Pigeonite clast 10	Augite lamellae	Augite grains	Silica polymorph	Shock melt veins
SiO ₂	45.1 ± 1.3	45.9 ± 1.9	49.0 ± 2.8	49.7 ± 0.9	51.4 ± 0.3	50.3 ± 1.2	51.3 ± 0.9	98.6 ± 1.5	48.0 ± 0.7
Al ₂ O ₃	34.9 ± 0.8	34.0 ± 1.5	32.9 ± 2.1	0.39 ± 0.23	0.62 ± 0.13	0.75 ± 0.18	0.38 ± 0.03	0.52 ± 0.64	19.3 ± 2.3
CaO	18.1 ± 0.7	17.8 ± 0.5	16.3 ± 1.2	1.71 ± 1.80	2.10 ± 0.38	19.2 ± 1.8	18.7 ± 4.0	0.30 ± 0.37	13.0 ± 0.9
Na ₂ O	1.10 ± 0.25	0.88 ± 0.12	1.63 ± 0.21	b.d.	b.d.	0.05 ± 0.02	b.d.	b.d.	0.93 ± 0.15
MgO	b.d.	0.19 ± 0.20	b.d.	13.9 ± 0.5	18.4 ± 0.5	11.5 ± 0.2	11.6 ± 0.3	b.d.	5.32 ± 1.03
FeO	0.15 ± 0.14	1.01 ± 0.23	0.59 ± 0.08	32.1 ± 1.9	25.7 ± 0.7	16.4 ± 2.1	16.4 ± 4.1	0.52 ± 0.53	11.6 ± 1.8
K ₂ O	0.05 ± 0.02	0.05 ± 0.02	0.12 ± 0.04	b.d.	b.d.	b.d.	b.d.	b.d.	0.06 ± 0.02
Cr ₂ O ₃	b.d.	b.d.	b.d.	0.48 ± 0.80	0.28 ± 0.20	0.83 ± 0.66	0.42 ± 0.26	b.d.	0.17 ± 0.05
MnO	b.d.	b.d.	b.d.	1.03 ± 0.08	0.83 ± 0.04	0.53 ± 0.07	0.56 ± 0.11	b.d.	0.38 ± 0.06
TiO ₂	b.d.	b.d.	b.d.	0.19 ± 0.10	0.13 ± 0.03	0.44 ± 0.42	0.15 ± 0.05	0.17 ± 0.39	0.76 ± 0.33
Total	99.5 ± 0.4	99.9 ± 0.8	100.6 ± 0.5	99.5 ± 0.6	99.5 ± 0.5	99.9 ± 1.0	99.6 ± 0.5	100.2 ± 0.7	99.5 ± 0.6
n	67	13	3	57	7	7	5	20	19
	An _{89.8 ± 2.5}	An _{91.5 ± 1.1}	An _{84.1 ± 3.0}	En _{42.2 ± 0.9}	En _{53.6 ± 1.4}	En _{33.2 ± 0.4}	En _{33.9 ± 1.2}		
	Ab _{9.85 ± 2.40}	Ab _{8.19 ± 1.04}	Ab _{15.2 ± 2.7}	Fs _{55.5 ± 1.4}	Fs _{42.0 ± 1.0}	Wo _{42.4 ± 1.0}	Wo _{39.2 ± 8.0}		
	Or _{-0.3}	Or _{-0.3}	Or _{-0.7}	Wo _{2.38 ± 1.32}	Wo _{4.3 ± 9.0.80}	Fs _{24.4 ± 0.9}	Fs _{26.9 ± 6.9}		

b.d. = below detection limits.

n = number of analyses (also equals the number of investigated grains except for the megaclasts; 10 megaclasts of both plagioclase and pyroxene were examined).

Table 1b. Chemical composition of oxide phases in DaG 983 (av. ox%).

	Chromite ^a	Ilmenite
SiO ₂	0.26 ± 0.17	0.19 ± 0.21
Al ₂ O ₃	8.1 ± 0.4	b.d.
CaO	0.07 ± 0.05	0.05 ± 0.05
MgO	0.52 ± 0.08	0.73 ± 0.06
FeO	34.6 ± 0.8	45.2 ± 0.3
Cr ₂ O ₃	51.7 ± 1.3	0.45 ± 0.60
MnO	0.83 ± 0.04	0.94 ± 0.03
TiO ₂	2.76 ± 0.93	51.0 ± 0.7
Total	98.8 ± 0.4	98.6 ± 0.4
n	32 (15)	39 (21)

^aUsp₃₁₋₃₅ with Usp = mol% ulvöspinel Fe₂TiO₄; Chm₃₈₋₃₉ with Chm = mol% chromite FeCr₂O₄.

b.d. = below detection limits.

n = number of analyses (number of investigated grains).

Table 2. Elemental concentrations of DaG 983.

	Sample splits			Average
	174.0 mg	147.4 mg	185.0 mg	
Na	2950	3780	3590	3440
Mg	3.9	6.2	4.1	4.7
Al	6.85	8.29	8.03	7.72
K	221	289	254	255
Ca	6.67	8.14	8.03	7.61
Sc	22.57	33.50	27.60	27.89
Ti	2600	4300	4300	3733
V	61	107	73	80
Cr	2023	3490	2606	2706
Mn	3360	5330	3890	4193
Fe	10.80	17.36	13.06	13.74
Co	14.24	11.69	7.82	11.25
Ni	30	<30	23	27
Ga	2.1	2.0	2.6	2.2
As	0.067	<0.11	0.085	0.076
Br	0.18	0.14	0.18	0.17
Rb	2.4	<4	<2.6	2.4
Sr	79.0	104	100	94.3
Zr	51.0	69.0	67.0	62.3
Ru	1.00	0.96	0.76	0.91
Sb	0.015	0.029	<0.014	0.022
La	2.36	3.29	3.07	2.907
Ce	5.84	8.38	7.53	7.25
Nd	4.9	6.7	5.3	5.6
Sm	1.392	1.987	1.79	1.723
Eu	0.546	0.67	0.689	0.635
Tb	0.346	0.5	0.453	0.433
Dy	0.30	0.30	0.23	0.28
Tm	1.37	2.04	1.75	1.72
Yb	0.203	0.296	0.266	0.255
Lu	0.87	1.37	1.38	1.21
Hf	0.46	0.28	0.21	0.32
Os	<0.004	0.004	0.004	0.004
Ir	0.001	<0.001	0.001	0.001
Au	0.30	0.42	0.30	0.34
Th	0.124	0.158	0.122	0.135
U	0.30	0.30	0.23	0.28

Concentrations are in g/g except for Mg, Al, Fe, Ca (%). Uncertainties are 1–5% for Na, Al, K, Ca, Sc, Cr, Mn, Fe, Co, La, Sm, Eu, Yb, Lu; 6–10% for Mg, V, Ce, Hf, Th, Mg; 11–20% for Ga, Sr, Ru, Sb, Ba, Nd, Tb, U; 21–30% for Ti, Ni, As, Br, Rb, Zr, Tm, Ta, Ir, Au.

fragments showing the typical subophitic texture of noncumulate eucrites. In addition, the sample contains patches of primary mesostasis (late stage interstitial igneous material). In modal terms, DaG 983 contains about 47 vol% pyroxene, 34% plagioclase, 12% melt, 3.5% silica, 1.5% ilmenite, 1.0% chromite as well as accessory phosphates and troilite.

Megacrystals

The majority of the pyroxene and plagioclase megacrystals measure 0.5 to 1.5 mm; the largest are up to 10 mm in diameter. The plagioclase crystals often exhibit numerous μm to sub- μm sized inclusions of pigeonite, augite,

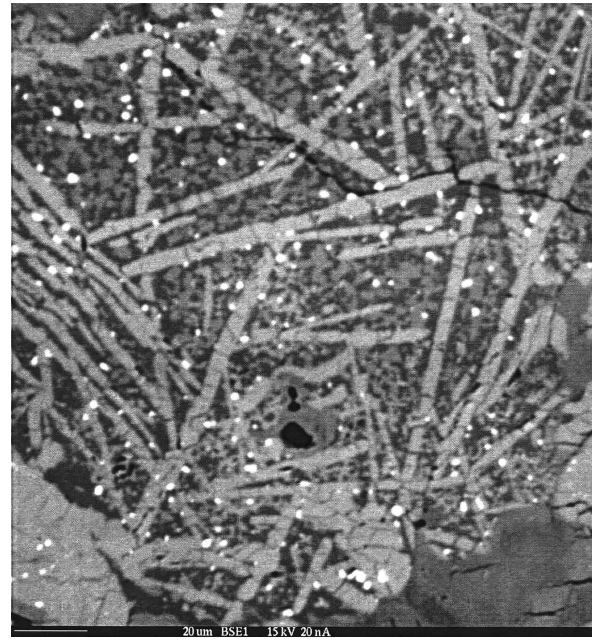


Fig. 2. Backscattered electron image of a melt pocket with spinifex-like texture in DaG 983 (scale bar = 20 μm). The texture of this particular melt clast was established upon quenching. Pyroxene (light grey) crystallized as fine needles. Plagioclase (medium grey) forms tiny anhedral to subhedral crystals in a silica rich matrix. White-colored spheres are opaque minerals.

chromite, silica, and troilite. Sometimes, they are oriented and elongated. Inclusions identified in the mega-pyroxenes are chromite with variable Ti concentrations and augite. In many cases, the pyroxene megacrystals also show fine augite exsolution lamellae.

Additional Clast Types

DaG 983 also contains two types of recrystallized melt. On one hand, we observed round pockets of fine crystalline subhedral plagioclase, pigeonite, and augite. Augite occurs as fine exsolution bands or discrete grains. Other phases can be silica and opaque minerals. The second type of melt clasts displays a spinifex-like texture indicating rapid cooling (Fig. 2). These quenched melt clasts consist of fine, up to $\sim 80 \mu\text{m}$ long pyroxene needles protruding into a silica-rich phase. Plagioclase is present as tiny crystals floating in the silica matrix. Small spheres of opaque minerals are variable in abundance. In addition to the recrystallized melt clasts, we detected basaltic clasts. They show the typical fine to medium grained subophitic texture known for many noncumulate eucrites. The pyroxene exhibits very fine and dense exsolution textures. In one example, we observed a pyroxene crystal that split and drifted apart to make room for expanding plagioclase laths (Fig. 3). This textural detail implies turbulent crystallization conditions similar to those inferred for the noncumulate eucrite DaG 872 (Patzer et al. 2003b).

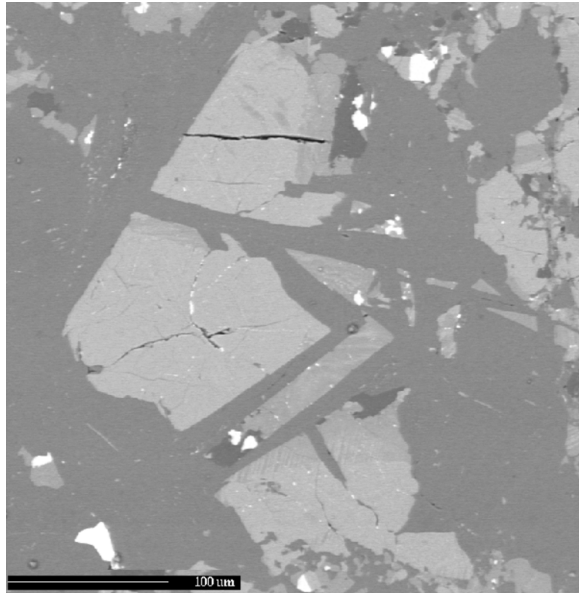


Fig. 3. Pigeonite crystal (center, light grey) surrounded by plagioclase (medium grey) that shows evidence for turbulent crystallization conditions. Pyroxenes generally precipitate from a melt earlier than plagioclase. The fragmentation of the pigeonite grain and filled-in plagioclase document a dynamic period during cooling of the basaltic parent magma (scale bar = 100 micrometers).

Matrix

All clasts identified in DaG 983 are embedded in a resolidified fragmental groundmass (Fig. 4). The main constituents of this matrix are plagioclase and pyroxene. Grain sizes vary widely from <10 to ~300 μm . Many pyroxene fragments display exsolution lamellae (augite of <1 to ~10 μm in width), often with dislocation or deformation features (kinking). In at least one occasion, twinning (herringbone texture) has been observed. Individual augite crystals (fragments) are also present. They sometimes reveal fine exsolution lamellae of orthopyroxene. In addition, we detected multiple chains of opaque droplets within the pyroxene crystals. This feature has been referred to as pyroxene clouding (Harlow and Klimentidis 1980) and is considered to be a form of exsolution as well (e.g., Arai et al. 1998).

The groundmass of DaG 983 also embodies patches of Si-rich mesostasis. They are of irregular shape and usually include abundant tiny droplets of opaque phases as well as fewer inclusions of plagioclase and pyroxene. In some cases, they are interconnected with pigeonite and plagioclase in a spongy or highly anhedral fashion.

Opaque Phases

Opaque minerals in DaG 983 are ilmenite and chromite. Troilite is rare and only occurs as tiny inclusions in some plagioclase megacrysts, mesostasis, and melt pockets. Chromite is present as individual crystals (typically <100 μm , up to 400 μm across) or in close association with ilmenite.

The chromite-ilmenite assemblages often display complex intergrowth textures. Pure ilmenite grains show diameters of up to 200 μm . They exist interstitially, like chromite, or are part of relatively coarse-grained polymineralic assemblages chiefly made of ilmenite and plagioclase, pyroxene, and silica.

Melt Veins

Glassy melt veins and patches can be found throughout the thin section. Appearance and texture vary. Some melt veins cut through plagioclase megacrysts or run along grain boundaries and contain numerous assimilated fragments of surrounding minerals. Others exist as irregular sub-millimeter-sized inclusions in some plagioclase megacrystals. A relatively large, sub-centimeter sized area of silica, associated with anhedral plagioclase and containing abundant ilmenite inclusions, is partly invaded by a dendritic network of porous melt patches.

A particularly interesting feature of DaG 983 are large pigeonites (200 μm and bigger) that appear to be “frozen” in the middle of a phase transformation process (Fig. 5). The pyroxenes in question seem to have turned into silica along with plagioclase and opaque inclusions. The transformation exhibits a very irregular pattern propagating from the center of the crystal toward its rims. The silica patches that are closely associated with highly anhedral pigeonite, plagioclase, and droplets of opaque minerals as described above may represent a later stage of this reaction.

Mineral Chemistry

Megacrystals

The monomineralic megacrysts are made of either calcic plagioclase or pigeonite (Table 1a). Calcium concentrations of the plagioclase megacrystals are fairly homogeneous but vary from grain to grain ($\text{An}_{81.8-93.6}$ over 10 clasts examined). With respect to Na, clasts 2 and 9 turn out to be more sodic ($\text{Ab}_{13.8 \pm 1.8}$) than all other megacrysts ($\text{Ab}_{9.0 \pm 1.4}$; Fig. 6). Zoning only occurs in clast 8. It displays decreasing Na concentrations toward its center.

The general lack of zoning and the relatively even distribution of Ca in plagioclase megacrysts suggest crystallization in a regime close to chemical equilibrium. This is consistent with the clast size (sub-centimeter), which, in turn, resulted from slow cooling. Variable Ca concentrations from clast to clast may be due to different crystallization times. Early precipitates contain relatively more anorthite leading to decreasing Ca concentrations of the melt with dropping temperatures. Sodium (albite) abundances are inversely correlated to this trend. Alternatively, the variations in Ca and Na contents may indicate sampling of distinct source magmas.

Nine out of ten pyroxene (pigeonite) megacrysts show a relatively homogeneous, Fe-rich composition ($\text{En}_{40.4-44.5}$)

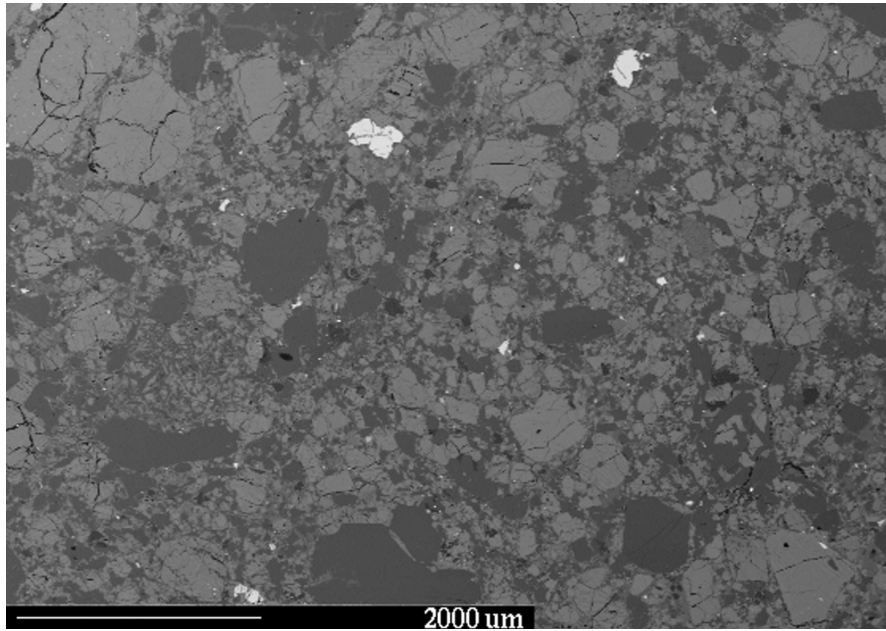


Fig. 4. Overview of DaG 983 showing the fragmental groundmass, plagioclase (dark grey) and pyroxene (medium grey) megacrysts as well as large and small opaque minerals (individual chromites and ilmenites and chromite-ilmenite assemblages in light grey; scale bar = 2 mm).

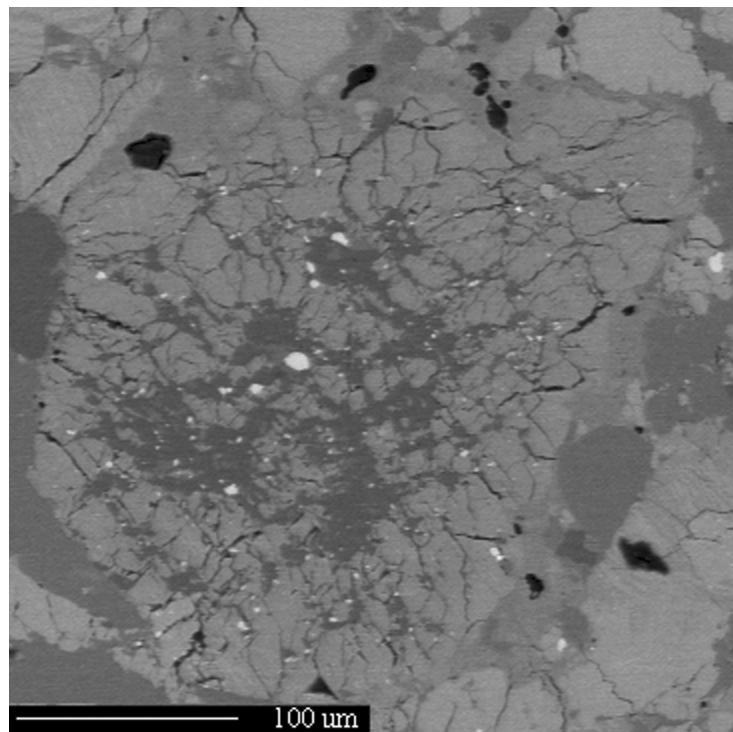


Fig. 5. Backscattered electron image of a pyroxene crystal that appears to display a disintegration reaction (scale bar = 100 μm). As DaG 983 exhibits phenomena of severe shock including deformation, strong mosaicism, maskelynitization of plagioclase, and shock melt veins, it is conceivable that some pyroxenes suffered incipient melting during the impact event.

with ferrosilite contents similar to those observed for noncumulate eucrites (e.g., Mittlefehldt et al. 1998). Magnesium numbers (mg#) average 43.6 ± 1.4 . Clast 10 displays relatively high Mg concentrations ($\text{En}_{52.3-55.5}$; Fig. 7,

Table 1a) with an average mg# of 56.1 ± 1.2 . This is similar to that reported for the cumulate eucrite Serra de Magé (mg# 55, Harlow et al. 1979). It may imply an earlier crystallization within the same cumulate pyroxene layer or an origin distinct

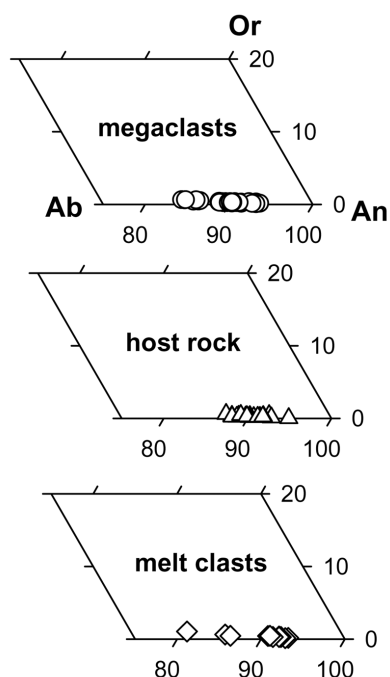


Fig. 6. A cut-out of the plagioclase ternary diagram illustrating the compositions of plagioclase in the megacrasts, host rock, and different melt clasts of DaG 983. All feldspars are generally Ca-rich. Relatively small-scale variations in the anorthite (An) and albite (Ab) contents testify to distinct spatial and/or temporal origins (Or = orthoclase).

from that of all other megacrystals. Three of the investigated crystals (including clast 10) also seem to have retained igneous zoning with Fe concentrations decreasing from rim to core. The occurrence of fine augite exsolution lamellae ($Wo_{41.0-43.6}$) is not uncommon.

Additional Clast Types

Two different types of recrystallized melt clasts are present in DaG 983. They can be distinguished with respect to their textures as well as their plagioclase composition (Fig. 6, Table 1a). Based on the observed differences, we infer distinct origins for both types of melt clasts. Plagioclase and pyroxene compositions in the clasts of subophitic basalt fall into the common range reported for noncumulate eucrites (e.g., Mittlefehldt et al. 1998).

Matrix

Compositions of plagioclase and pigeonite of the fragmental groundmass are like those of megacrasts and subophitic mineral components (Figs. 6 and 7, Table 1a). Moderate chemical variations observed among the fragmental feldspars may be due to primary magmatic zoning (e.g., Yamaguchi et al. 1996, 1997b) and/or the turbulent crystallization conditions as deduced from textural evidence (see above).

Unlike augite exsolution lamellae, discrete augite grains

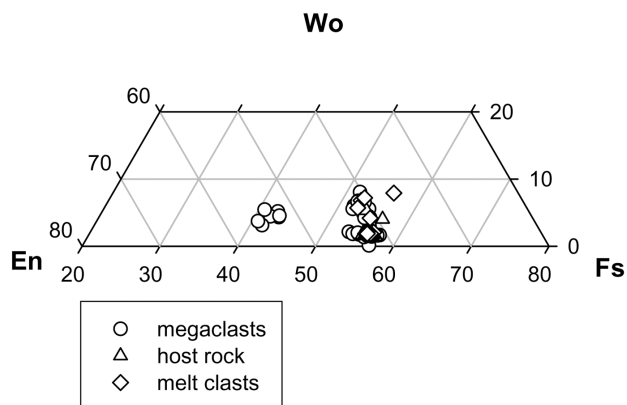


Fig. 7. A cut-out of the pyroxene ternary diagram depicting the compositions of pyroxene in the megacrasts, host rock, and different melt clasts of DaG 983. Most pyroxenes (pigeonites) show similar En (enstatite), Fs (ferrosillite), and (Wo = wollastonite) contents. Only one of the ten megacrystals examined yields a more Mg-rich composition suggesting an earlier precipitation than the other pyroxene megacrystals. Alternatively, it could originate from a different intrusive body.

of the matrix feature a comparatively broad range of Ca and Fe contents ($Wo_{26.8-45.3}Fs_{22.3-37.7}$; Table 1a). It is conceivable that the Ca-rich and, by inference, Fe-poor augites precipitated at an earlier stage of the crystallization sequence than those enriched in Fe and low in Ca.

Opaque Phases—Chromites

Individual chromites in DaG 983 and those intergrown with ilmenite may represent one generation as they all show similar compositions (Table 1b). Absolute Ti contents and mg# are comparatively low and yield values similar to those determined for the polymict eucrite Y-791192 (Mittlefehldt and Lindstrom 1993). Chromite inclusions in the pyroxene megacrystals turn out to be compositionally distinct from their single grain equivalents. They show significantly higher Mg, and particularly Al, concentrations (~0.8 wt% Mg and ~8.0 wt% Al versus ~0.3 wt% and 4.3 wt%, respectively).

Recent surveys of the texture and composition of spinels in basaltic eucrites suggest that the Ti concentration is indicative of the metamorphic temperature experienced (Arai et al. 1998; Yamaguchi 2000). Arai et al. (1998) suggest that Ti-rich spinels might emerge during high temperature annealing. Ti contents of the chromites in DaG 983 are relatively low. Based on observations by Yamaguchi (2000) and in accordance with Arai et al. (1998), this may hint at a comparably low stage of equilibration (pigeonites of type 4). When applying the classification scheme of Takeda and Graham (1991), noncumulate pigeonites of DaG 983 qualify as metamorphic types 3 and 4. Thus, the approach of Yamaguchi (2000) of assessing equilibration in eucritic meteorites via the Ti content of chromites is consistent with the established method of Takeda and Graham (1991). Alternatively, the chromites in DaG 983 may simply represent

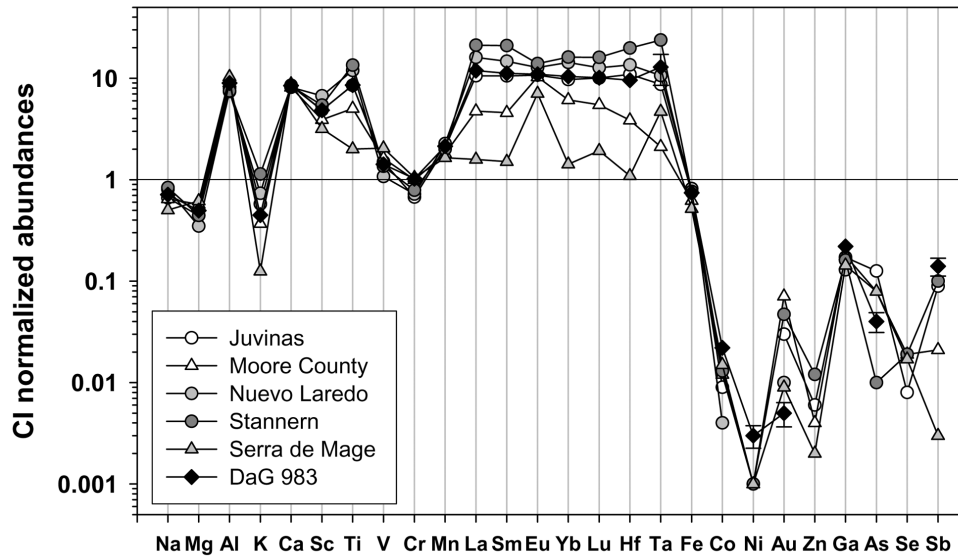


Fig. 8. DaG 983 shows relative abundances of lithophile elements similar to those of the noncumulate eucrite Juvinas including a flat REE pattern at about $10 \times$ CI (data from Kitts and Lodders 1998). The order of elements is based on geochemical group (lithophiles: Na–Ta, siderophiles: Fe–Au, chalcophiles: Zn–Sb) and atomic number.

early primary crystallization products (versus a late precipitation that would have been reflected by higher Ti concentrations) (El Goresy, personal communication).

The agreement of Ti contents in chromites with the equilibration state of the pyroxenes in the groundmass suggests that both minerals were part of a single noncumulate eucritic parent rock. The clasts of mesostasis and subophitic basalt may stem from the same source rock as well.

Opaque Phases—Ilmenite

With the exception of Cr, the elemental concentrations of all analyzed ilmenites match closely (Table 1b). Cr concentrations tend to be higher in those ilmenites that are closely associated with chromite. A systematic trend as a function of distance from the adjacent chromite crystal could not be determined due to small crystal sizes of the ilmenite-chromite assemblages.

In addition to ilmenite-chromite intergrowths, we detected small grains and droplets of ilmenite in patches of mesostasis as well as large assemblages that contain major ilmenite, silica, and plagioclase. Both occurrences are late-stage igneous products due to the incompatibility of Ti. Individual, up to 200 μm in size, ilmenite crystals might have formed after the growth of chromite and chromite-ilmenite but before the late-stage assemblages.

Melt Veins

The chemical composition of the ubiquitous melt veins and patches in DaG 983 is as heterogeneous as expected (Table 1a). On average, however, it probably matches the bulk composition of the meteorite (Metzler et al. 1995). In this context, it appears noteworthy that some elemental

abundances of the melt associated with the sub-centimeter-sized silica area are considerably different from the average. Sodium concentrations are clearly higher (1.31 wt% versus 0.69 wt% in the average melt) and Mg and Fe concentrations are lower (1.23 wt% versus 3.21 wt% and 3.96 wt% versus 8.97 wt%, respectively). The Si content, on the other hand, turns out to be only insignificantly higher. The chemical discrepancy is therefore unlikely to be caused by the admixture of silica melt. Instead, a higher fraction of plagioclase melt may account for the difference. We suggest that the melt was completely injected into the silica area upon impact rather than being produced in situ.

INAA Data

Noncumulate eucrites are basaltic rocks that consist primarily of pyroxene and plagioclase. Relative to CI chondrites, their elemental distribution patterns are characterized by high concentrations of refractory incompatible lithophile elements including rare earth elements (REEs). Chalcophiles and particularly siderophiles occur in relatively low concentrations. Plagioclase typically shows a high anorthite component. The pyroxenes are usually more ferroan than magnesian.

Cumulate eucrites basically follow the same compositional trend, being relatively enriched in refractory incompatible lithophile elements and depleted in siderophiles and chalcophiles. Key chemical differences include more magnesian pyroxenes and more calcic plagioclase. With respect to the REE, noncumulate eucrites are known to display flat distribution patterns at high abundances (~ 10 – $20 \times$ CI) whereas the cumulate eucrites exhibit diagnostic

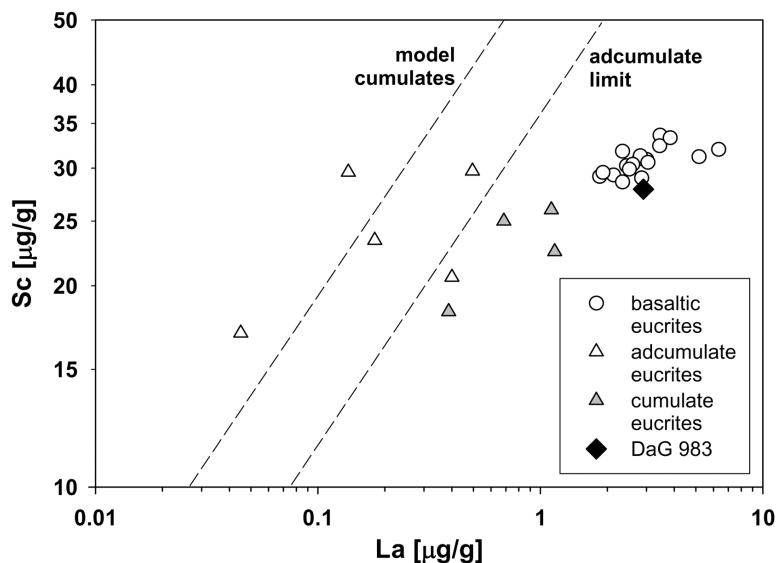


Fig. 9. Noncumulate, adcumulate, and cumulate eucrites are distinguishable on the basis of their Sc and La concentrations (data from Kitts and Lodders 1998; MetBase 2000; Mittlefehldt and Lindstrom 2003; dashed lines indicating the adcumulate limit and model cumulate compositions are taken from Mittlefehldt and Lindstrom 2003). Sc is slightly incompatible only in pyroxene whereas La is incompatible in both pyroxene and plagioclase. Consequently, La tends to exhibit higher concentrations in cumulate eucrites (which contain a certain amount of melt component) than it does in quasi melt-free adcumulate eucrites. Basaltic eucrites yield the highest La contents. For DaG 983, Sc and La abundances are apparently dominated by the elemental inventory of the fragmental matrix, which is of noncumulate origin.

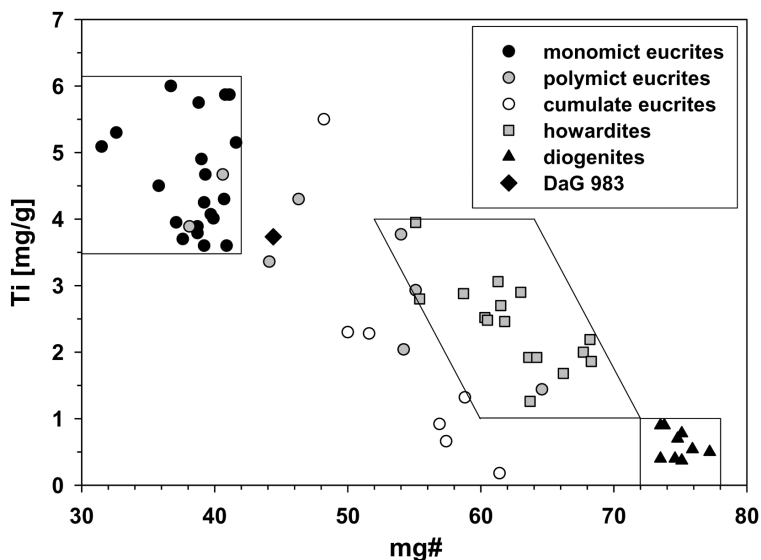


Fig. 10. Howardites, eucrites, and diogenites can be discriminated by comparing their individual bulk Ti concentrations and mg# (Mittlefehldt 1979; data from MetBase 2000). DaG 983 plots separately from the basaltic eucrites and reveals similarities to the polymict and cumulate eucrites. Thus, some bulk rock attributes of DaG 983 like the mg# and Ti abundance are consistent with the petrographic findings whereas the lithophile element pattern (Figs. 8 and 9) reflects the presence of a noncumulate eucritic component in this meteorite.

signatures with significantly lower concentrations ($1-5 \times \text{CI}$), positive Eu anomalies, and slight enrichments of HREEs.

DaG 983 shows the same relative abundances of lithophile elements that are observed for the noncumulate eucrite Juvinas (Fig. 8). In particular, it reveals the same flat REE pattern at an abundance level of about $10 \times \text{CI}$. Figure 9 illustrates the concentration of the highly incompatible trace element Sc as a

function of (incompatible) La. Mittlefehldt and Lindstrom (2003) used a Sc versus La diagram to distinguish noncumulate eucrites from adcumulate as well as cumulate eucrites that contain variable amounts of trapped melt. Again, DaG 983 plots with the basaltic eucrites. Based on bulk INAA data, DaG 983 appears to belong to the group of basaltic eucrites, which is in contrast to the petrographic findings.

Other efforts to graphically separate noncumulate from cumulate eucrites include the CaO content, mg# (molar MgO/[MgO + FeO]), and Ti concentrations. Grossman et al. (1981) showed that howardites, eucrites, and diogenites occupy different areas in a diagram of CaO versus mg#. Likewise, HED meteorites can be differentiated by comparing Ti concentrations and mg# of individual HED meteorites (Fig. 10). Following these approaches, DaG 983 is unambiguously allocated apart from the monomict eucrites and falls into the range of polymict and cumulate eucrites. This agreement concurs with the petrographic results of our study.

Noble Gas Data

Investigating the cosmic ray exposure ages (CREA) of HED meteorites, Eugster and Michel (1995), Shukolyukov and Begemann (1996), and Welten et al. (1997) found convincing support for the hypothesis that these meteorites originated from the same planetary body. Based on clusters in the exposure age distribution pattern, they also concluded that the HED parent body experienced several significant impact events, two of which result in major clusters at about 22 and 38 Ma.

A detailed survey on the noble gas record of DaG 983 has been given by Patzer et al. (2003a). In brief, DaG 983 yields a T_{21} of 15.7 ± 2.4 Ma and may be linked to the exposure age cluster of HED defined at 14 ± 1 Ma (Shukolyukov and Begemann 1996). As to the shielding conditions, DaG 983 reveals little shielding that occurred either on a very small meteoroid or near the surface of a bigger body resulting in a relatively high cosmogenic $^{22}\text{Ne}/^{21}\text{Ne}$ ratio of 1.226.

CONCLUSIONS

The lithological constituents identified in DaG 983 appear to sample possibly three different rock types of the HED parent body. We found pyroxene and plagioclase megacrystals whose compositions are consistent with an origin from an intrusive complex on the HED parent body. Chemical differences within each group of megacrystals represent either distinct layers of the sampled intrusion or different cumulate bodies. Furthermore, we detected a variety of minerals and clasts of a noncumulate eucrite source, and possibly melt clasts of a third parent rock. In addition, the textural and chemical diversity of individual components in DaG 983 allows us to reconstruct the meteorite's evolutionary history. We suggest the following sequence of events in order to explain the observed petrographic attributes:

1. Crystallization of primary magmas took place.
2. An intense series of impact events (Bogard 1995) penetrates basaltic surface and cumulate subsurface layers of the HED parent body and results in the formation of a thoroughly mixed megaregolith (Metzler

and Stöffler 1987; Metzler et al. 1995; Takeda 1997). Fragmentation and deformation of rock components occur. Melt veins and pockets are generated. Subsequent quenching induces the creation of spinifex-like textures in some melt pockets.

3. A phase of moderate reheating follows. The brecciated parent rock of DaG 983 is consolidated. Upon slow cooling, exsolution of pyroxene is triggered. The small width of augite exsolution lamellae in both the cumulate and noncumulate pigeonites is consistent with their growth under relatively low temperatures (Boctor et al. 1994). In addition, formerly glassy melt clasts now recrystallize to fine-grained equigranular pockets of pyroxene and plagioclase. The thermal overprinting may be induced by hot impact melt sheets or hot impact breccias in a crater contact zone according to the scenarios described by Nyquist et al. (1986) and Metzler et al. (1995).
4. Finally, the DaG 983 polymict eucrite is expelled by a major impact event that also induces mosaicism, maskelynitization of plagioclase, and impact melting. Some pyroxenes that now show signs of decomposition are possibly affected by partial melting. In addition, radiogenic ^4He and primordial trapped rare gases are released. The U/Th-He retention age is completely reset. The production of cosmogenic nuclides commences (see Patzer et al. 2003a). The impact that liberated the DaG 983 meteoroid took place approximately 15 Ma ago, in conjunction with the production of numerous other HED meteoroids. Shielding of the DaG 983 sample was low, suggesting that either the respective meteoroid was a small, cm-sized body or DaG 983 occupied a close-to-surface position of a bigger meteoroid (Patzer et al. 2003a).
5. After its fall in the Libyan desert, DaG 983 is exposed to terrestrial alteration for a significant amount of time. Weathering is recognized by calcite and gypsum precipitates in cracks and also leaves its mark on the noble gas inventory of the meteorite.

Acknowledgments—The DaG 983 meteorite was recovered with the valuable help of the expedition participants Friedhelm Thiedig (Hamburg, Germany) and Abd Elfatah M. Abu-Aghreb (Tripoli, Libya). The expedition was made possible by the German Science Foundation (SCHL 549/1-2), the Max-Planck-Institution (Germany), and the Industrial Research Center (Libya). The analytical work carried out in Tucson at the Lunar and Planetary Laboratory of the University of Arizona benefited from technical assistance by K. Domanik and was supported by NASA grant NAG5-4944. Thorough reviews by D. Mittlefehldt and the associate editor, M. Caffee, as well as constructive comments by D. Garrison and T. McCoy indubitably helped improve the original manuscript.

Editorial Handling—Dr. Marc Caffee

REFERENCES

- Arai T., Takeda H., Lofgren G. E., and Miyamoto M. 1998. Metamorphic transformation of opaque minerals in some eucrites. *Antarctic Meteorite Research* 11:71–91.
- Boctor N. Z., Palme H., Spettel B., El Goresy A., and McPherson G. J. 1994. Caldera: A second unbreciated noncumulate eucrite (abstract). *Meteoritics* 29:A445.
- Bogard D. D. 1995. Impact ages of meteorites: A synthesis. *Meteoritics* 30:244–268.
- Basaltic Volcanism Study Project. 1981. *Basaltic volcanism on the terrestrial planets*. New York: Pergamon Press. 1286 p.
- Clayton R. N. and Mayeda T. K. 1996. Oxygen isotopes studies of achondrites. *Geochimica et Cosmochimica Acta* 60:1999–2017.
- Drake M. J. 2001. The eucrite/Vesta story. *Meteoritics & Planetary Science* 36:501–513.
- Eugster O. and Michel T. 1995. Common asteroid breakup events of eucrites, diogenites, and howardites and cosmic-ray production rates for noble gases in achondrites. *Geochimica et Cosmochimica Acta* 59:177–199.
- Grossman L., Olsen E., Davis A. M., Tanaka T., and MacPherson G. J. 1981. The Antarctic achondrite ALH A76005: A polymict eucrite. *Geochimica et Cosmochimica Acta* 45:1267–1279.
- Harlow G. E. and Klimentidis R. 1980. Clouding of pyroxene and plagioclase in eucrites: Implications for post-crystallization processing. Proceedings, 11th Lunar and Planetary Science Conference. pp. 1131–1143.
- Harlow G. E., Nehru C. E., Prinz M., Taylor G. J., and Keil K. 1979. Pyroxenes in Serra de Magé: Cooling history in comparison with Moama and Moore County. *Earth and Planetary Science Letters* 43:173–181.
- Kitts K. and Lodders K. 1998. Survey and evaluation of eucrite bulk compositions. *Meteoritics & Planetary Science* 33:A197–A213.
- Kring D. A., Swindle T. D., Britt D. T., and Grier J. A. 1996. Cat Mountain: A meteoritic sample of an impact-melted asteroid regolith. *Journal of Geophysical Research* 101:29353–29371.
- Jörn Koblitz. MetBase 2000. Version 5.0 for Windows. Meteorite data retrieval software. Fischerhude, Germany.
- Metzler K. and Stöffler D. 1987. Polymict impact breccias on the eucrite parent body: I. Lithic clasts in some eucrites and howardites (abstract). 18th Lunar and Planetary Conference. pp. 641–642.
- Metzler K., Bober K. -D., Palme H., Spettel B., and Stöffler D. 1995. Thermal and impact metamorphism of the HED parent body. *Planetary and Space Sciences* 43:499–525.
- Mittlefehldt D. W. and Lindstrom M. M. 1993. Geochemistry and petrology of a suite of ten Yamato HED meteorites. *Proceedings of the NIPR Symposium on Antarctic Meteorites* 6:268–292.
- Mittlefehldt D. W. and Lindstrom M. M. 2003. Geochemistry of eucrites: Genesis of basaltic eucrites, and Hf and Ta as petrogenetic indicators for altered Antarctic meteorites. *Geochimica et Cosmochimica Acta* 67:1911–1935.
- Mittlefehldt D. W., McCoy T. J., Goodrich C. A., and Kracher A. 1998. Non-chondritic meteorites from asteroidal bodies. In *Planetary materials*, edited by Papike J. J. Washington, D.C.: Mineralogical Society of America. pp. 4-1–4-195.
- Nyquist L. E., Takeda H., Bansal B. M., Shih C.-Y., Wiesmann H., and Wooden J. L. 1986. Rb-Sr and Sm-Nd internal isochron ages of a subophitic basalt clast and a matrix sample from the Y-75011 eucrite. *Journal of Geophysical Research* 91:8137–8150.
- Nyquist L. E., Bogard D., Takeda H., Bansal B. M., Wiesmann H., and Shih C.-Y. 1997. Crystallization, recrystallization, and impact-metamorphic ages of eucrites Y-792510 and Y-791186. *Geochimica et Cosmochimica Acta* 61:2119–2138.
- Patzer A., Schultz L., and Franke L. 2003a. New noble gas data of primitive and differentiated achondrites including NWA 011 and Tafassasset. *Meteoritics & Planetary Science* 38:1485–1497.
- Patzer A., Hill D. H., and Boynton W. V. 2003b. New eucrite Dar al Gani 872: Petrography, chemical composition, and evolution. *Meteoritics & Planetary Science* 38:783–794.
- Patzer A., Hill D. H., and Boynton W. V. 2004. Evolution and classification of acapulcoites and lodranites from a chemical point of view. *Meteoritics & Planetary Science* 39:61–85.
- Pouchon J. L. and Pichoir F. 1991. Quantitative analysis of homogenous or stratified microvolumes applying the model “PAP.” In *Electron probe quantitation*, edited by Heinrich K. F. J. and Newbury D. E. New York: Plenum Press. pp. 31–75.
- Russell S. S., Zipfel J., Folco L., Jones R., Grady M. M., McCoy T., and Grossman J. N. 2003. The Meteoritical Bulletin No. 87. *Meteoritics & Planetary Science* 38:A189–A248.
- Schlüter J., Schultz L., Thiedig F., Al-Mahdi B. O., and Abu Aghreb A. E. 2002. The Dar al Gani meteorite field (Libyan Sahara): Geological setting, pairing of meteorites, and recovery density. *Meteoritics & Planetary Science* 37:1079–1093.
- Shukolyukov A. and Begemann F. 1996. Cosmogenic and fissiogenic noble gases and ⁸¹Kr-Kr exposure age clusters of eucrites. *Meteoritics & Planetary Science* 31:60–72.
- Stöffler D., Bischoff A., Buchwald V., and A. E. Rubin 1988. Shock effects in meteorites. In *Meteorites and the early solar system*, edited by Kerridge J. F. and Matthews M. S. Tucson, Arizona: The University of Arizona Press. pp. 165–201.
- Stolper E. M. 1977. Experimental petrology of eucritic meteorites. *Geochimica et Cosmochimica Acta* 41:587–611.
- Takeda H. 1997. Mineralogical records of early planetary processes on the howardite, eucrite, diogenite parent body with reference to Vesta. *Meteoritics & Planetary Science* 32:841–853.
- Takeda H. and Graham A. L. 1991. Degree of equilibration of eucritic pyroxenes and thermal metamorphism of the earliest planetary crust. *Meteoritics* 26:129–134.
- Tschermak G. 1885. *Die mikroskopische Beschaffenheit der Meteoriten*, edited by Koch E. Stuttgart: Ernst Schweizerbart'sche Verlagsbuchhandlung. 24 p.
- Welten K. C., Lindner L., van der Borg K., Loeken T., Scherer P., and Schultz L. 1997. Cosmic-ray exposure ages of diogenites and the recent collisional history of the howardite, eucrite and diogenite parent body/bodies. *Meteoritics & Planetary Science* 32:891–902.
- Yamaguchi A. 2000. Spinels in basaltic eucrites: Implications for crystallization and metamorphic history (abstract). *Meteoritics & Planetary Science* 35:A174.
- Yamaguchi A., Taylor G. J., and Keil K. 1996. Global crustal metamorphism of the eucrite parent body. *Icarus* 124:97–112.
- Yamaguchi A., Taylor G. J., and Keil K. 1997a. Metamorphic history of the eucritic crust of 4 Vesta. *Journal of Geophysical Research* 102:13381–13386.
- Yamaguchi A., Taylor G. J., and Keil K. 1997b. Shock and thermal history of equilibrated eucrites from Antarctica. *Proceedings of the NIPR Symposium on Antarctic Meteorites* 10:415–436.
- Yamaguchi A., Taylor G. J., and Keil K. 2001. Post-crystallization reheating and partial melting of eucrite EET 90020 by impact into the hot crust of asteroid 4 Vesta ~4.50 Ga ago. *Geochimica et Cosmochimica Acta* 65:3577–3599.